Measuring the basal melt rate of Antarctic ice shelves using GPS and phase-sensitive radar observations

Adrian Jenkins, Hugh Corr, Keith Nicholls, Chris Doake and Craig Stewart
British Antarctic Survey, Natural Environment Research Council,
High Cross, Madingley Road, Cambridge, CB3 0ET, U.K.

Introduction

Basal melting of Antarctica's floating ice shelves accounts for between 15 and 35% of the total mass loss from the ice sheet and helps to precondition the shelf waters for deep convection. Despite this pivotal role in ice sheet-ocean interactions, there are only a handful of measurements of actual melting rates. Almost all published figures are of steady state melt rates; that is, the melt rate required to maintain the ice shelf in a state of equilibrium, deduced from the residual of the other mass balance terms. Such observations have obvious limitations, such as the impossibility of determining the role of basal melting in driving ice shelf thinning or retreat. Over the past two Antarctic field seasons we have conducted a series of experiments to measure the actual melt rate at various locations on George VI and Filchner-Ronne ice shelves. The key to our technique is a precise measurement of the ice shelf thinning rate, by phase-sensitive radar. The thinning rate can be partitioned between vertical strain and melting without the need to assume that the ice shelf is in equilibrium, given contemporaneous measurements of the vertical strain rate.

Theory

Applying the principle of mass conservation to a moving column of ice on an ice shelf we obtain:

$$\frac{DH_r}{Dt} + H_r\left(\frac{\partial u}{\partial x} + \frac{\partial v}{\partial y}\right) + \frac{m_s}{n_i}\left(\frac{1}{\rho(h_u)} - \frac{1}{\rho_i}\right) = -\frac{m_b}{\rho_i}$$

where H_r is the effective ice thickness derived from measurement of the two-way travel time of a radar pulse transmitted through the ice shelf and an assumption of constant refractive index, n_i, and m_s and m_b are surface and basal mass fluxes, defined as positive for a downwards mass flux. Other symbols have their conventional meanings, with the subscript *i* indicating values for solid ice. In deriving the above expression, we have made the conventional assumption that the density varies only with depth below the surface and is otherwise spatially and temporally constant, and have made use of the fact that the refractive index of ice and firn is linearly related to density. We have also assumed that the thickness is measured between an internal radar reflector, which we have taken to be a material surface, and the ice shelf base. The term $\rho(h_u)$ refers to the density at the depth of this upper reflecting horizon. If the upper reference horizon is deep enough to lie within solid ice, the last term on the left-hand side is identically zero; otherwise the size of this last term, which physically results from compaction beneath the reference depth, must be estimated.

We can apply this same equation to the thickness, H_{ri}, measured between two internal reflectors, and if these are both within the solid ice below the firn layer and are both material

surfaces, we arrive at a simple expression for the horizontal divergence term that appears above:

$$\left(\frac{\partial u}{\partial x}+\frac{\partial v}{\partial y}\right)=-\frac{1}{H_{ri}}\frac{DH_{ri}}{Dt}$$

Making use of the above two equations we can derive the basal melt rate of an ice shelf directly from repeat radar sounding. If two suitably deep internal reflectors are not available the horizontal divergence can be measured separately by the repeat survey of a pattern of surface markers.

Method

The practical application of the technique is illustrated in Figure 1. At the start of the experiment a column of ice was marked and the thickness between a prominent internal radar reflector and the ice shelf base was measured. Each thickness measurement actually comprised six individual soundings, spaced at short intervals, to ensure the correct identification of stable internal reflectors. The radar was a step frequency system (Corr et al., 2002) configured to respond as an equivalent pulsed system having a centre frequency close to 300 MHz and a bandwidth of between 60 and 160 MHz. Since both the amplitude and phase of the radar signal were recorded, changes in the range of reflectors could be measured to a small fraction (~1%) of the wavelength, giving sub-centimetre accuracy on the ice thickness changes. Survey poles were set in the snow surface around the site of the radar sounding, and inter-stake distances were measured using GPS techniques. The stake pattern was triangular to provide measurements of extension or compression in three directions. Trimble 4000 series GPS receivers were use to record dual frequency, carrier phase data. FastStatic™ processing techniques then yielded inter-stake distances to ~1 cm or better with observation times as short as 8-10 min. The survey was designed so that all the required inter-stake distances were directly-observed GPS baselines, ensuring no degradation of accuracy through the need to infer distances from the measured coordinates of the (moving) survey markers.

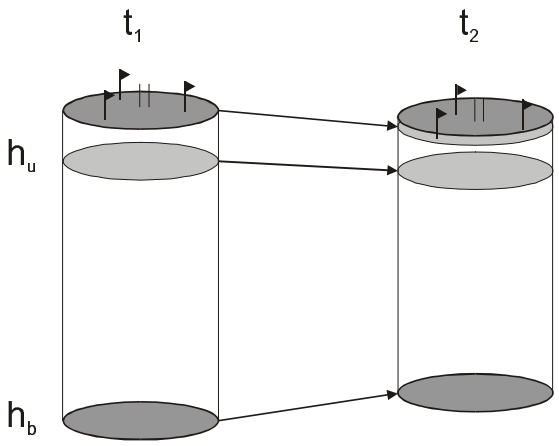

Figure 1: Ice column at times t_1 and t_2. Repeat observations of (h_u-h_b) are made. The rate at which this quantity changes is determined by horizontal convergence/divergence of the ice flow, measured by repeat survey of surface markers, and basal melting/freezing.

On subsequent visits all the measurements were repeated. The initial and repeat radar soundings provided the ice thickness and material derivative of thickness that appear in the above equations. Given a suitable selection of internal radar reflectors these were the only measurements that needed to be made. Where the observable internal layering did not extend deep enough, we estimated the parameters in the compaction term from regional surface accumulation and temperature data. We also used the results of the GPS surveys to deduce the horizontal divergence term. Where both radar and GPS measurements of the latter were available, we favoured the former, this being a point measurement on the ice column of interest rather than an areal average over a finite region surrounding the radar site.

Most of the sites discussed here (Figure 2) were established in the austral summer of 2000/01, with repeat visits being made that summer over periods ranging from a few days up to one month. Some of these sites were revisited in 2001/02, giving estimates of year-round melting, and further sites were established, for which only summer (2002) melt rates are so far available.

Results

Time-series measurements on George VI Ice Shelf and Rutford Ice Stream

At both these locations (see map) the radar sites were visited repeatedly during the course of the initial survey. These experiments provide the best estimate of the true precision of the thickness change measurements, taking into account not only the performance of the radar but also the errors associated with repositioning the system over the same column of ice. Likely errors in positioning are ~1 cm over short periods, but probably rise to ~10 cm over the year-long observations.

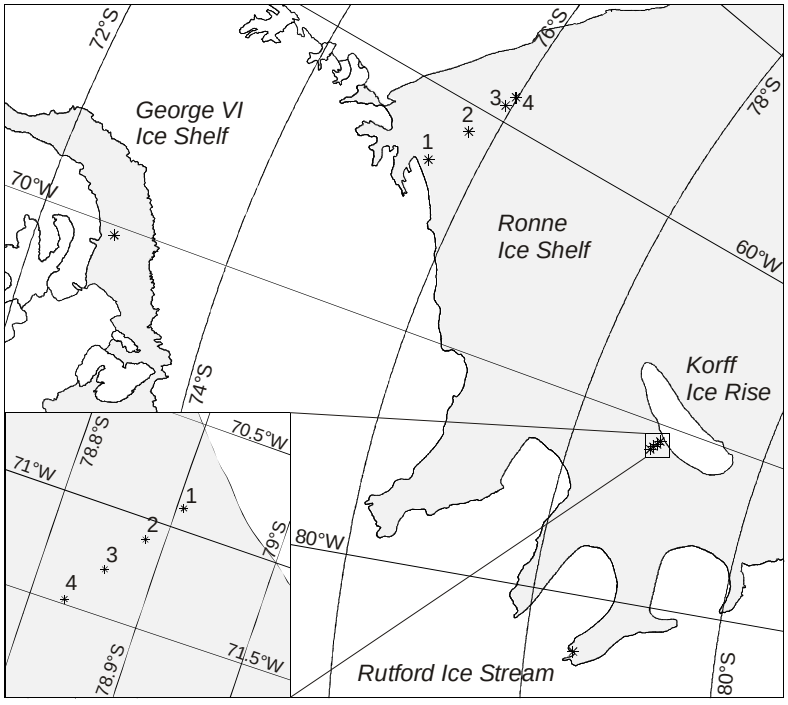

Figure 2: Map showing the location of the measurement sites discussed in the text (black stars). Floating ice is shaded.

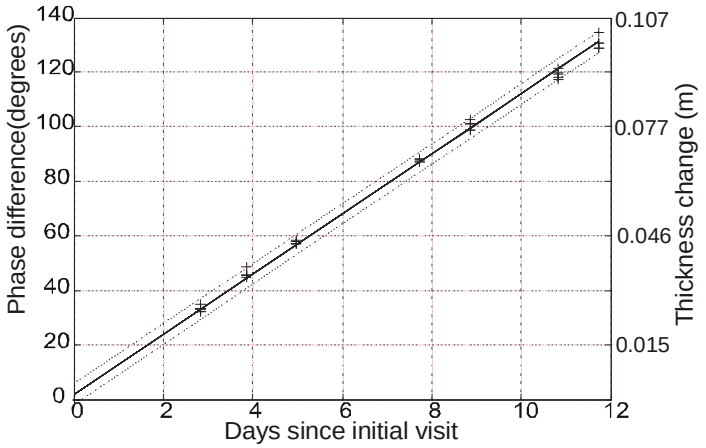

Figure 3: Thickness change observed over a twelve-day period on George VI Ice Shelf. The scales indicate the position of the ice shelf base relative to its initial depth, i.e. the ice column is thinning. Dotted lines are two standard deviations above and below the best fit (solid) line.

Figure 3 shows the results from nine observations (each comprising six individual thickness soundings) at S72° 47' 41", W070° 20' 16" on George VI Ice Shelf. The data are displayed as a change in phase of the return signal, and the equivalent change in path length, from that of the original measurement. The standard deviation about the best fit straight line is 2° of phase, equivalent to 1.5 mm of ice. Once the contributions of compaction and horizontal divergence have been taken into account, the observed thinning rate implies basal melting at a rate of 2.78±0.08 m yr^{-1} over the twelve-day period (Corr et al., 2002). This is somewhat higher than the regional average equilibrium melt rate, calculated by Potter and Paren (1985) as 2.17±0.14 m yr^{-1}. Since melting in this region is driven by the inflow of warm Circumpolar Deep Water, which has a fairly constant temperature year-round, we would not anticipate a large seasonal variation in the basal melting.

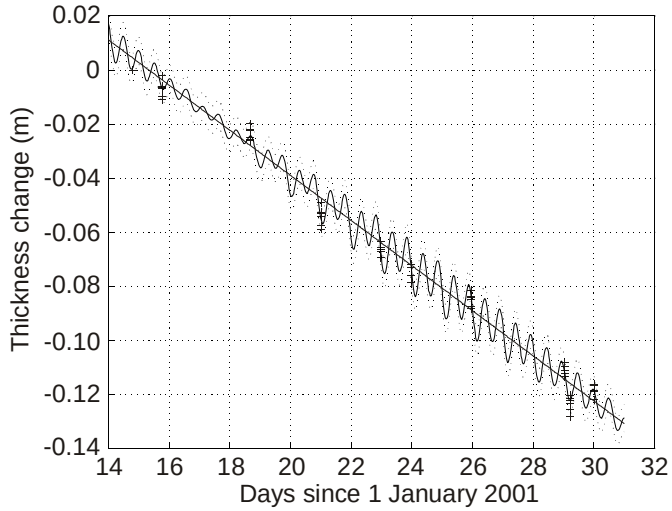

Figure 4: Thickness change observed over a fifteen-day period on Rutford Ice Stream. The scales indicate the position of the ice shelf base relative to its initial depth, i.e. the ice column is thickening. Dotted lines are two standard deviations above and below the best fit (solid) line. The straight, solid line indicates the thickening trend with the tidal component removed.

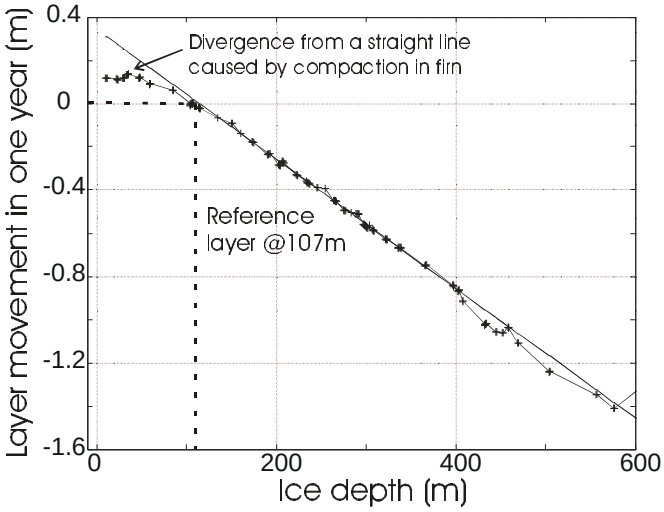

Figure 5: Annual displacement of internal layers relative to a reference horizon at 107 m depth plotted as a function of initial depth. The gradient of the straight line fit gives the vertical strain over one year. Layer movement is down with respect to the reference indicating that the ice column is undergoing vertical extension. In the surface layers the extension is offset by compaction of the firn.

A similar set of measurements, made at S78° 30' 24", W082° 58' 08", a few kilometres downstream of the grounding line on Rutford Ice Stream, are plotted in Figure 4. In this case ten sets of six thickness soundings were recorded over a period of fifteen days. The standard deviation about the best fit straight line in this case is 5 mm of ice. Although the spread within the individual groups of six measurements is clearly larger than in the previous example the grouping is suggestive of some systematic variations in thickness, which were found to correlate with the tidal height. Fitting the observations to a linear trend plus a constant factor times the predicted tidal height (Figure 4) reduces the standard deviation to around 2.5 mm and implies tidal variations in thickness that have a maximum range of just over 2 cm during the spring tides that occur around day 24.

The linear trend implies a thickening rate of 3.05±0.03 m yr^{-1} during the fifteen-day timespan of the initial observations. The site was revisited a year later and two further observations of thickness were made. Over the "full" year (333 days) we find a thickening rate of 3.05±0.02 m yr^{-1}, suggesting no seasonal variation in the melt rate. From the relative displacement of the internal layers observed between depths of 100 and 600 m over the "full" year, we obtain a vertical strain rate of (2.90±0.01) x 10^{-3} yr^{-1} (Figure 5). The ice column here is under horizontal compression, so that the ice between 100 m depth and the ice shelf base would thicken at a rate of 4.23±0.01 m yr^{-1} in the absence of melting. The difference between this and the measured thickening rate implies a basal melt rate of 1.18±0.03 m yr^{-1}. In Figure 5 the effect of firn compaction, which balances horizontal compression near the surface, can clearly be seen in the relative displacement of the layers above 100 m. This value for the melt rate is remarkably close to the steady state melt rate of 1.2±0.5 m yr^{-1} calculated by Jenkins and Doake (1991) for the same site. The closeness of these two values is probably fortuitous, given that the downstream advection of ice thickness anomalies in this region is known to induce localised non-steady behaviour, but does illustrate that the measured melt rate is consistent with broad-scale equilibrium of the ice stream in the vicinity of its grounding line.

Spatial and temporal pattern of melting near the coast of Korff Ice Rise

Four separate sites were established at 5 km intervals along a line approximately perpendicular to the coast of Korff Ice Rise (Figure 2). The location of Site 3 coincided with that of an oceanographic mooring site (also Site 3), set up in January 1996 (Nicholls and Makinson, 1998). Radar measurements have been made at each site on three occasions: once when they were set up in early January 2001, again in early February 2001, and once more in late December 2001. The melt rates measured over one month and one year at each site are shown in Table 1.

Table 1: Melt rates calculated at sites near Korff Ice Rise (Figure 2).

Site	Ice depth (m)	Time diff (days)	Melt rate (m yr^{-1})	Error (m yr^{-1})
Korff 1	783	31.9	0.87	0.02
		350.8	0.83	0.003
Korff 2	802	31.2	0.73	0.02
		350.0	0.59	0.003
Korff 3	816	36.7	0.78	0.02
		350.7	0.56	0.003
Korff 4	821	31.8	0.68	0.02
		347.9	0.43	0.003

The most striking feature of these numbers is that melting rates are significantly above the year-round average during the summer (January) at all sites. The reason for this is apparent in the record of ocean temperature recorded at Site 3 (Nicholls and Makinson, 1998). The oceanographic data are not contemporaneous with the radar measurements, but subsequent observations suggest that the phasing of the annual cycle in water temperature does not vary much from year to year. The highest temperatures throughout the water column are observed between November and March, and coincide with the arrival in this part of Ronne Depression of High Salinity Shelf Water (HSSW) that was generated at the Ronne Ice Front during the previous winter.

Another obvious feature of the figures in Table 1 is the generally decreasing melt rate with increasing distance from the coast, which might be explained by upwelling of the warm, inflowing HSSW at the coast. In general, an ice shelf thins in the direction of flow, so, if the upper layers of the underlying seawater are freshened by melt, the isopycnal surfaces in the ocean should slope up quasi-parallel to the ice shelf base. This should promote current shear in the water column perpendicular to the direction of ice flow, with the upper part flowing to the left (looking in the direction of ice flow) and the lower part flowing to the right. Such motion would cause upwelling at a coast lying on the right-hand side (looking in the direction of ice flow), such as the western coast of Korff Ice Rise, and downwelling at a coast on the left. Such an explanation of the spatial pattern of melting near Korff Ice Rise is consistent with the finding of Makinson (2002) that tidally-induced vertical mixing in the water column at Site 3 is insufficient to supply the heat needed to melt the ice shelf at the inferred rate (somewhat less than the observed rate reported here). Makinson (2002) concluded that most of the heat must therefore be supplied by advection within the ice-ocean boundary layer. The increasing seasonality of the melting with increasing distance from the coast could also be explained through this mechanism. The increased flow of HSSW during the November to March period could lead to stronger upwelling and more efficient advection of the heat away from the site of coastal upwelling.

Spatial pattern of melting on north-west Ronne Ice Shelf

In the austral summer of 2001/02, four radar sites were established ~50 km south of the Ronne Ice Front, spanning the Ronne Depression. They were reoccupied 2-3 weeks following their establishment. Two of them (sites 1 and 4) were situated (unwittingly) on the downstream end of the two westernmost bodies of marine ice that form in the flow shadows of Fowler Peninsula and Cape Zumberge. At site 1 the ice shelf base could not be unambiguously detected, but at site 4 a weak basal return was observed through what appears to be about 60 m of marine ice. At sites 2 and 3 strong returns were found, consistent with a pure ice-water basal interface at these locations. The derived melt rates for the three sites with identifiable basal returns are given in Table 2.

Table 2: Melt rates calculated at sites on north-west Ronne Ice Shelf (Figure 2).

Site	Ice depth (m)	Time diff (days)	Melt rate (m yr^{-1})	Error (m yr^{-1})
NW Ronne 2	365	15.7	0.12	0.04
NW Ronne 3	398	19.1	0.00	0.04
NW Ronne 4	334	15.0	1.41	0.08

Site 4 is about 40 km to the west of the penultimate site on the flowline studied by Jenkins and Doake (1991). At the time of their study this site was about the same distance from the ice front as the north-west Ronne sites are from the current ice front. Jenkins and Doake (1991) estimated a steady state melt rate of 1.6±0.5 m yr^{-1} at their site, consistent with the recent findings at site 4. However, distance from the ice front is clearly not the only factor determining the melt rate, as the sharp decline to near zero melting west of site 4 indicates. The controlling factor is most likely the route taken by the inflowing HSSW, which is likely to follow the eastern side of Ronne Depression and therefore pass directly beneath site 4. Models typically show stronger melting on the eastern side of the depression (Gerdes et al., 1999; Jenkins and Holland, 2002a,b), and the channel of thinner ice that extends in from the ice front here (note the difference in thickness between sites 3 and 4) is probably a result of this. Observations at the ice front typically show Ice Shelf Water dominating much of Ronne Depression, and if this water mass occupies the water column beneath sites 2 and 3, near-zero melting is perhaps not surprising. It will be interesting to see if such low melt rates are only a summer feature, with higher melting during winter when the inflow of HSSW becomes more vigorous, but further observations at these sites are required before that question can be answered.

Conclusions

We have described an experimental technique whereby the melt rate at the base of an ice shelf can be measured at high spatial and temporal resolution. Compared with traditional techniques used to estimate steady state melt rates, these observations provide new insight into the processes operating in the ocean beneath Antarctica's ice shelves.

Our observations of melting on Ronne Ice Shelf are broadly consistent with earlier estimates of steady state melting, suggesting that the regions we have studied are close to equilibrium. On George VI Ice Shelf our measured melt rate was significantly higher than the regional average steady state melt rate. However, the limited scope of our observations (this was primarily a test site for the technique) means that we are unable to ascribe this difference to either spatial or temporal variability in melting or to thinning of the ice shelf.

Data from the interior of Ronne Ice Shelf suggest proximity to a southern or eastern boundary implies relatively high melting and suppressed seasonality. These observations are consistent with a picture in which localised upwelling near the boundaries and horizontal advection of heat away from the upwelling sites supplies the heat to fuel basal melting over large areas, rather than one in which the heat is supplied by more uniform and widespread vertical diffusion. In contrast, our observations from nearer the ice front, which show high melt rates above the location of a deep inflow of HSSW, seem more consistent with the latter picture, with the heat for melting presumably being supplied locally by vertical diffusion. Tides probably provide the energy for enhanced vertical mixing here, because the eastern side of Ronne Depression lies on the western boundary of a region characterised by high tidal dissipation rates (Makinson and Nicholls, 1999), owing to the relatively shallow water column and strong tidal currents. Although strong vertical mixing is not in itself sufficient to generate high melt rates, the position of site 4 over the HSSW inflow would appear to guarantee a ready supply of ocean heat. It is probable that the sharp transition to lower melting to the west of north-west Ronne site 4 results from a combination of just lower water temperatures and a marked decrease in vertical mixing. Further observations at these sites, and in particular the installation of oceanographic instruments to monitor the water column should help to clarify the source of the high spatial gradients in basal melting.

References

Corr, H.F.J., A. Jenkins, K.W. Nicholls and C.S.M. Doake. 2002. Precise measurement of changes in ice-shelf thickness by phase-sensitive radar to determine basal melt rates, *Geophys. Res. Lett.*, **29**(8), 10.1029/2001GL014618.

Gerdes, R., J. Determann and K. Grosfeld. 1999. Ocean circulation beneath Filchner-Ronne Ice Shelf from three-dimensional model results, J. Geophys. Res., 104(C7), 15,827–15,842.

Jenkins, A. and C.S.M. Doake. 1991. Ice-ocean interaction on Ronne Ice Shelf, Antarctica, J. Geophys. Res., 96(C1), 791–813.

Jenkins, A. and D.M. Holland. 2002a. A model study of circulation beneath Filchner-Ronne Ice Shelf, Antarctica: Implications for bottom water formation, *Geophys. Res. Lett.*, **29**(8), 10.1029/2001GL014589.

Jenkins, A. and D.M. Holland. 2002b. Correction to "A model study of circulation beneath Filchner-Ronne Ice Shelf, Antarctica: Implications for bottom water formation" by Adrian Jenkins and David M. Holland, *Geophys. Res. Lett.*, **29**(13), 10.1029/2002GL015647.

Makinson, K. 2002. *Tidal Currents and Vertical Mixing Processes beneath Filchner-Ronne Ice Shelf*, Ph.D. Thesis, Open University, xxiv+208 pp.

Makinson, K. and K.W. Nicholls. 1999. Modeling tidal currents beneath Filchner-Ronne Ice Shelf and on the adjacent continental shelf: their effect on mixing and transport, *J. Geophys. Res.*, **104**(C6), 13,449–13,465.

Nicholls, K.W. and K. Makinson. 1998. Ocean circulation beneath the western Ronne Ice Shelf, as derived from in situ measurements of water currents and properties, in *Ocean, Ice and Atmosphere: Interactions at the Antarctic Continental Margin*, edited by S.S. Jacobs and R.F. Weiss, *Antarct. Res. Ser.*, **75**, 301–318.

Potter, J.R. and J.G. Paren. 1985. Interaction between ice shelf and ocean in George VI Sound, Antarctica, in *Oceanology of the Antarctic Continental Shelf*, edited by S.S. Jacobs, *Antarct. Res. Ser.*, **43**, 35–58.